ORIGINAL ARTICLE   **Open Access**

Three-Dimensional Numerical Study on the Metal Rotating Spray Transfer Process of High-Current GMAW

Lei Xiao[1,2,3], Ding Fan[2*] and Jiankang Huang[3*]

Abstract

A three-dimensional numerical model based on the volume-of-fluid (VOF) method is typically preferred for studying high-current gas metal arc welding (GMAW) metal transfer mechanism and then controlling it. It is informed that the rotating spray transfer is extremely complicated, and some researchers have focused on simplified models without considering the energy conservation to make analysis manageable for the unstable metal transfer process. Using our created numerical model, the metal transfer of high-current GMAW with shielding gas of different conductivities has been studied by analyzing acting forces and fluid flows in the metal liquid column, especially for the contributions of the self-induced electromagnetic force, equivalent volume force of the capillary pressure of the surface tension (Named surface tension force in this work), static arc pressure. It is found that the unbalanced electromagnetic force greatly promotes the metal rotating motion in 500 A metal inert gas (MIG) welding with pure argon shielding gas and it pushes the metal liquid column to rotate. Considering the arc constricting effect in active shielding gas by simply changing the arc conductivity, it is found that the metal liquid column no longer rotates, it turns to swing since the unbalanced electromagnetic force is large enough to break the rotating motion. The calculated results of the metal liquid column deflected angle and rotating/swing frequency agree well with the experiment of high-speed camera observations.

Keywords: Gas metal arc welding, Rotating spray transfer, Three-dimensional model, Electromagnetic force, Surface tension

1 Introduction

Increasing welding efficiency is under large significance for shortening the producing/processing time since welding is indispensable in most of the manufacturing processing. To acquire a high-efficiency GMAW process of large travel speed and melting rate, increasing the welding current in the feeding wire is a less complicated and more effective way. In the meantime, the metal transfer process will change from globular transfer to spray transfer. The project and stream spray transfers are widely used in the high-quality welding process. However, rotating spray transfer is avoided in most welding industrial applications because of its spatter deficiency [1]. As the environmental issue has become the main problem in recent years, the environmental protection of welding spatters and fume in the welding processes is going to be more and more significant [2]. Some control methods including the magnetic field control methods [3, 4] and altered voltage wave control methods [5] were ultimately attempted to reduce the spatter in high-current GMAW. Nevertheless, the acting mechanism of main forces in the rotating metal liquid column was not clear on account of its complication. It

*Correspondence: fand@lut.cn; sr2810@163.com

[2] State Key Laboratory of Advanced Processing and Recycling of Non-ferrous Metals, Lanzhou University of Technology, Lanzhou 730050, China
[3] School of Materials Science and Engineering, Lanzhou University of Technology, Lanzhou 730050, China
Full list of author information is available at the end of the article

Xiao *et al. Chinese Journal of Mechanical Engineering*   (2022) 35:131

Page 2 of 13

is necessary to make the rotating mechanism understood and contribute to finding a way for controlling the unstable metal transfer process in high-current GMAW.

Electromagnetic forces in the molten metal are no doubt the strongest acting force when the welding current exceeds 400 A with a 1.2 mm diameter steel wire in GMAW. And it is difficult to measure the current density in the conductive region by experimental methods directly because of the high-temperature and small-size welding region. Hence numerical simulation method based on computational fluid dynamics (CFD) including the volume-of-fluid (VOF) method, which is investigated to be adaptable than the static equilibrium theory [6, 7] and varicose instabilities theory [8, 9], is advantaged to make it possible to estimate the electromagnetic force distributions and flow fields in the liquid phase. The acting forces in the metal liquid column include gravity, electromagnetic force, surface tension force, arc plasma shear stress, the opposing force caused by the metal evaporation, arc pressure, and positive pole spot pressure. Besides, their strengths alter at different welding parameters. It is not possible to accurately consider all the mentioned forces in a uniformed mathematic model, and the most viable way is to simplify the model by taking into account only the primary factors. Choi et al. [10] considered gravity, the electromagnetic force, and surface tension in the globular and spray transfer models, and fixed current density was assumed on the droplet surface which generated the prime acting force of self-induced electromagnetic force. Wang et al. [11] applied that method of setting current flux on the droplet surface to the pulsed GMAW. Wu et al. [12] modified the mathematic model to consider shear stress from arc plasma and assumed that the current density distribution in the droplet was Gaussian. Wang et al. [13] developed their model by assuming both current density distribution and heat flux distribution on the droplet surface, the shape of the melting interface on the welding wire was accurately predicted. Moreover, coupled models including arc and droplets have also been reported in recent years [14–19]. In the coupled models, the current density can be calculated by the coupled conservation equations, hence the calculated results are more accurate than previous simplified models. It is significant that the metal vapor behavior can be accurately expressed in the coupled model [20–22], and the sharp transition in the droplet size and detachment frequency when the metal transfer changes from globular to spray mode can also be observed in the coupled unified models [23, 24].

However, it is difficult to deal with the three-dimensional rotating transfer process of high-current GMAW by modeling an arc and metal liquid column coupled model since there are still some difficulties to deal with the coupled boundary between the gas phase and liquid phase. To solve this problem, Ogino et al. [25] proposed a three-dimensional metal transfer model considering gravity, surface tension, and electromagnetic force to study the metal transfer processes of different current GMAW. However, in their model, the arc plasma flow was ignored. It is no doubt that the arc pressure is large enough to impact the metal transfer process in high-current GMAW. In our present work, an upgraded three-dimensional model is proposed by considering both the metal flow and the arc plasma flow using two individual momentum balance equations. The metal transfer, variations of current density distributions, velocity vector fields, and electromagnetic force distributions in the molten metal liquid column in 500 A GMAW are analyzed. The metal liquid column rotating frequencies and deflected angles agree well with the verification of experimental results.

2 Mathematical Model

2.1 Assumptions

1. The arc is considered as a gas phase while the molten or solid wire is treated as a liquid phase. Both the gas and liquid phases are incompressible, Newtonian, and laminar flow [15, 26].
2. Only mass and momentum transfer processes are considered in this work. We assume constant conductivity, viscosity, density for argon plasma in this numerical model according to the argon plasma physical properties at 15000 K. It is a very rough treatment for arc conductivity, which is affected by the arc temperature field, flow field, metal vapor effects a lot [22]. However, it is a reasonably simple arc conductive mechanism referenced to Ref. [25], and it can also be applied in some other researches which have no concern with arc temperature.
3. Since the temperature field is not coupled in this work, the interactions between the liquid phase and the gas phase contain only forces and electrical potential. The anode sheath effects and metal vapor behavior are both ignored.

2.2 Conservation Equations

The unitive form of the governing equations is listed as follows:

$$\frac{\partial}{\partial t}(\rho \Phi) + \nabla \cdot (\rho \overrightarrow{v} \Phi) = \nabla \cdot (\Gamma_\Phi \nabla \Phi) + S_\Phi, \qquad (1)$$

where t is the time, ρ is the density, Φ is the generic variable, $\overrightarrow{v}$ is the velocity vector, Γ_Φ is the diffusion coefficient and S_Φ is the source term. Table 1 shows the details of the governing equations.

Table 1 The governing equations

Governing equations	Φ	Γ_Φ	S_Φ
Mass	1	0	0
Momentum	$\overrightarrow{v}$	μ	$-\nabla P + \overrightarrow{j} \times \overrightarrow{B} + \rho\overrightarrow{g}$
Electric field	V	σ	0
Magnetic field	$\overrightarrow{A}$	1	$\mu_0 \overrightarrow{j}$
VOF	F_{mp}	0	0

In Table 1, μ is the dynamic viscosity, P is the pressure, $\overrightarrow{j}$ is the current density, $\overrightarrow{B}$ is the magnetic flux density, $\overrightarrow{g}$ is the gravitational acceleration, V is the electrical potential, σ is the electric conductivity, $\overrightarrow{A}$ is the magnetic vector potential, μ_0 is the permeability of vacuum $(4\pi \times 10^{-7} \text{ H·m}^{-1})$, F_{mp} is the volume fraction of the metal liquid phase, and the volume fraction of gas-phase F_{gp} reads as follows:

$$F_{gp} = 1 - F_{mp}. \tag{2}$$

In the boundary region of the gas and liquid phase, the gas phase has a small density and large velocity while the liquid phase has a large density and small velocity. Therefore, laws of conservation of mass and momentum should be satisfied by each phase individually. The multi-fluid VOF model is used to calculate two independent momentum conservation equations of metal and gas phases and two independent mass conservation equations as well. The mixing phase properties for the density ρ_{mix}, the dynamic viscosity μ_{mix}, and the electrical conductivity σ_{mix} are defined by the volume fractions and properties of two phases, respectively.

$$\rho_{mix} = F_{gp}\rho_g + F_{mp}\rho_m, \tag{3}$$

$$\mu_{mix} = F_{gp}\mu_g + F_{mp}\mu_m, \tag{4}$$

$$\sigma_{mix} = F_{gp}\sigma_g + F_{mp}\sigma_m. \tag{5}$$

Two assisted equations about current density $\overrightarrow{j}$ and magnetic flux density $\overrightarrow{B}$ are added as follows:

$$\overrightarrow{j} = -\sigma(\nabla V) = \sigma\overrightarrow{E}, \tag{6}$$

$$\overrightarrow{B} = \nabla \times \overrightarrow{A}. \tag{7}$$

2.3 Boundary Conditions

Figure 1 displays the three-dimensional cylinder calculated domain and boundary conditions. The domain diameter is 24 mm, and the height is 12 mm with a wire
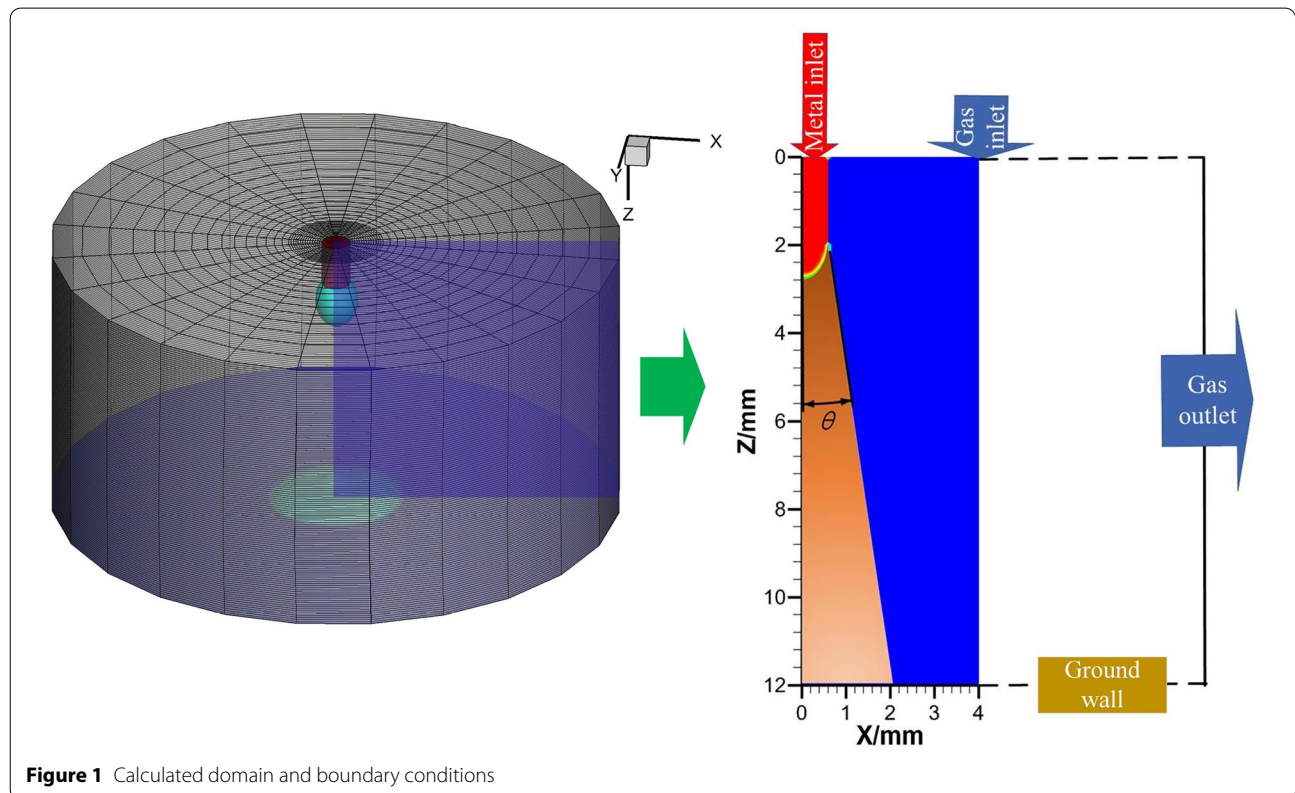

Figure 1 Calculated domain and boundary conditions

Xiao *et al. Chinese Journal of Mechanical Engineering*   (2022) 35:131

Page 4 of 13

length of 2 mm, an arc length of 10 mm. The metal flows into the arc region from the boundary of "metal inlet" while the shielding gas flows through the boundary of "gas inlet". There is an assumed arc disperse angle θ colored with orange, which is set to 20° according to the experimental high-speed observation of arc sharp and Ref. [25]. It has been studied that, polyatomic shielding gas like O_2, CO_2 can constrict the arc to the metal liquid column tip for it has higher specific heat and thermal conductivity, hence more current will flow through the molten metal. We define different conductivities in the arc region for approximately consider different shielding gases of pure argon shielding gas and CO_2 mixed with argon shielding gas.

Table 2 lists the external boundary conditions. All the metal part of the calculated region is assumed to be fluid injecting from the "metal inlet" boundary, and the flow velocity is 0.5 m/s, and so does the shielding gas flow rate. The arc plasma shear stress is modified to a body force by multiplying with the gradient of the volume fraction as follows:

$$\overrightarrow{\tau}_{ps} = \mu_g \frac{\partial \overrightarrow{v}}{\partial \overrightarrow{s}} \cdot \left| \nabla F_{mp} \right|, \tag{8}$$

where $\overrightarrow{s}$ is the tangential normal vector to the free surface. The Marangoni shear stress due to temperature variation is neglectable and the surface tension in the free surface region is considered as follows [27]:

$$\overrightarrow{F}_{st} = \gamma k_{cur} \nabla F_{mp}, \tag{9}$$

where $\overrightarrow{F}_{st}$ is the equivalent volume force vector of surface tension pressure, γ is the surface tension coefficient, k_{cur} is the curvature, calculated as follows:

$$k_{cur} = \nabla \cdot \frac{\nabla F_{mp}}{\left| \nabla F_{mp} \right|}. \tag{10}$$

2.4 Numerical Considerations and Initial Conditions
Commercial CFD software FLUENT is used in this work. Only structured meshes are applied in the whole calculated domain for easier convergences and more
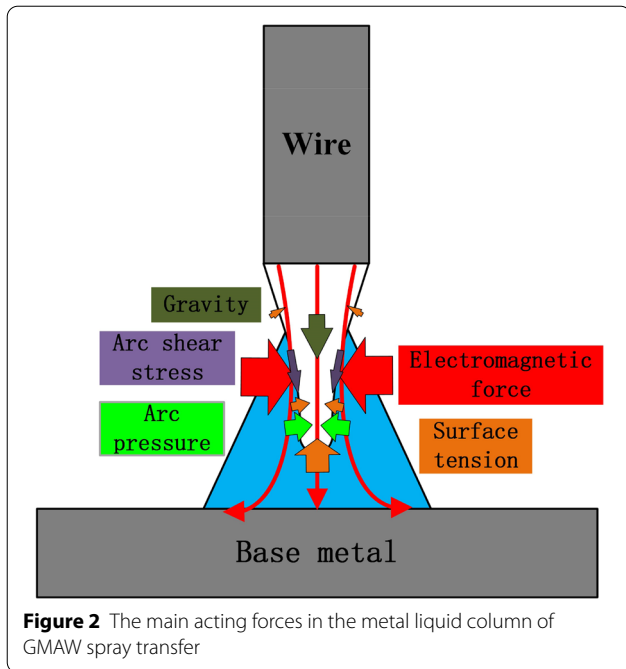
accurate results. There are more than 100000 meshes in the 5000 mm³ calculated domain. The finest mesh size is 0.05 mm in the metal transfer region. It was reported in Ref. [28] that, the mesh size should be larger than 0.1 mm for ignoring the non-LTE (Local Thermodynamic Equilibrium) region in the arc-droplet coupled model using "LTE-diffusion approximation". However, the heat transfer is not considered in this work, and the arc conductivity is set to constant, we can use a fine mesh for the accurately calculated process. A pressure-based solver and phase coupled SIMPLE (Semi-Implicit Method for Pressure Linked Equations) algorithm with second-order and high-resolution spatial discretization are applied. Nomura et al. [29] measured the welding arc temperature of more than 400 A spray transfer GMAW with the spectroscopic method, and it is reported that the arc temperature in the electric arc conductive region is around 13000–15000 K. For 500 A GMAW in this work, the density, dynamic viscosity, and electrical conductivity of the gas phase are chosen as the argon plasma physical and transfer properties at the temperature of 15000 K. For the non-arc region of the gas phase colored with blue, a relatively small value of about 10 S/m is set to forbid the current to flow through. The shielding gas flow rate is 20 L/min, and the welding current is 500 A. To approximately express the arc constricting to the tip of the metal liquid column, we assume the arc conductivity of Ar-CO_2 mixture shielding gas to be half of the pure argon shielding gas. In the results, we use Metal Inert Gas (MIG) and Metal Active Gas (MAG) to differentiate these two cases. This is a rough way to consider the influence of different shielding gases in GMAW, especially for high-current cases. However, considering the complexity of the three-dimensional arc-metal coupled model in recent times, we prefer this simplified model for an advanced look of the high-current rotating spray transfer process and its mechanism. A heat and mass transfer rotating spray model can be impelled based on this research.

3 Results and Discussions
The main acting forces in the molten metal liquid column are shown in Figure 2. They are all treated as volume forces with a unit of N/m³ besides the original volume forces of gravity, electromagnetic forces. Gravity and arc shear stress drive the metal to transfer no doubt. The electromagnetic force is a pinch force, which will pressure the metal to flow upward and downward respectively. Surface tension is related to the surface curvature of the metal liquid column, and it will be discussed for its shifty in one metal transfer period. The largest arc pressure acts on the metal surface where the arc velocity is lowest around the surface since the mathematic relation between arc pressure and arc velocity is an inverse

Table 2 External boundary conditions

Boundary	$\overrightarrow{v}$ (m·s^{-1})	P (Pa)	V (V)	$\overrightarrow{A}$ (Wb/m)
Gas inlet	v_g	P_{ATM}	$\frac{\partial V}{\partial n} = 0$	$\frac{\partial A_i}{\partial n} = 0$
Metal inlet	v_m	P_{ATM}	$-\sigma \frac{\partial V}{\partial n} = j$	$\frac{\partial A_i}{\partial n} = 0$
Gas outlet	$\frac{\partial (\rho v_i)}{\partial n} = 0$	–	$\frac{\partial V}{\partial n} = 0$	$A = 0$
Ground wall	No-slip	–	0	$\frac{\partial A_i}{\partial n} = 0$

$\overrightarrow{n}$: unit vector

Figure 2 The main acting forces in the metal liquid column of GMAW spray transfer

(a) MIG

(b) MAG

Figure 3 The metal transfer processes of 500 A MIG and MAG

proportion. The forces will change when the welding current increases to about 500 A for a 1.2 mm diameter wire, and we will study on it using our proposed 3D high-current GMAW metal transfer mathematical model.

3.1 Rotating Spray Transfer and Swing Spray Transfer

As shown in Figure 3, there are two different metal transfer modes. One is rotating spray transfer at the rotating frequency of about 500 Hz, and the other one is swing spray transfer at a swing frequency of about 400 Hz. The largest deflected angles of them respectively are 34° and 90°, hence the welding spatter in MAG is much more serious. The only distinction between MIG and MAG in our mathematical model is the arc conductivity. The arc conductivity in MAG is half of that in MIG, which will cause more current to flow through the metal liquid column instead of the arc region, and the arc constricts to the metal tip. The strengths of the gravity, surface tension force, electromagnetic force, arc pressure are different between MIG and MAG, which will be discussed in detail below.

There are apparent spatters during the transfer process. Observing at Figure 4, it is distinct that the spatter velocity reaches more than 5 m/s in both MIG and MAG cases, which will no doubt destroy the welding stability. The maximal velocity in the liquid phase exists near the bending point of the metal liquid column, where the curvature is the largest. There are many more spatters in the swing process of MAG since the deflected angle is larger than MIG. To explain the rotating and
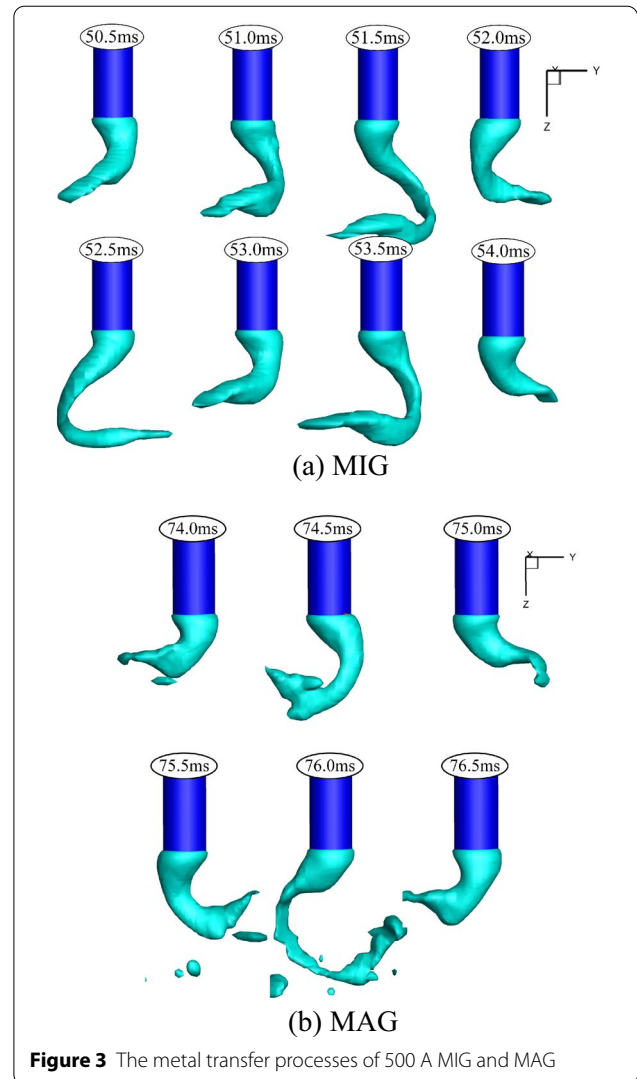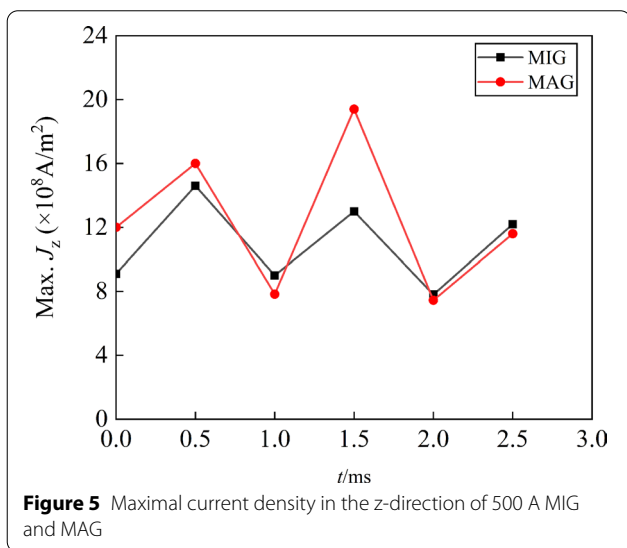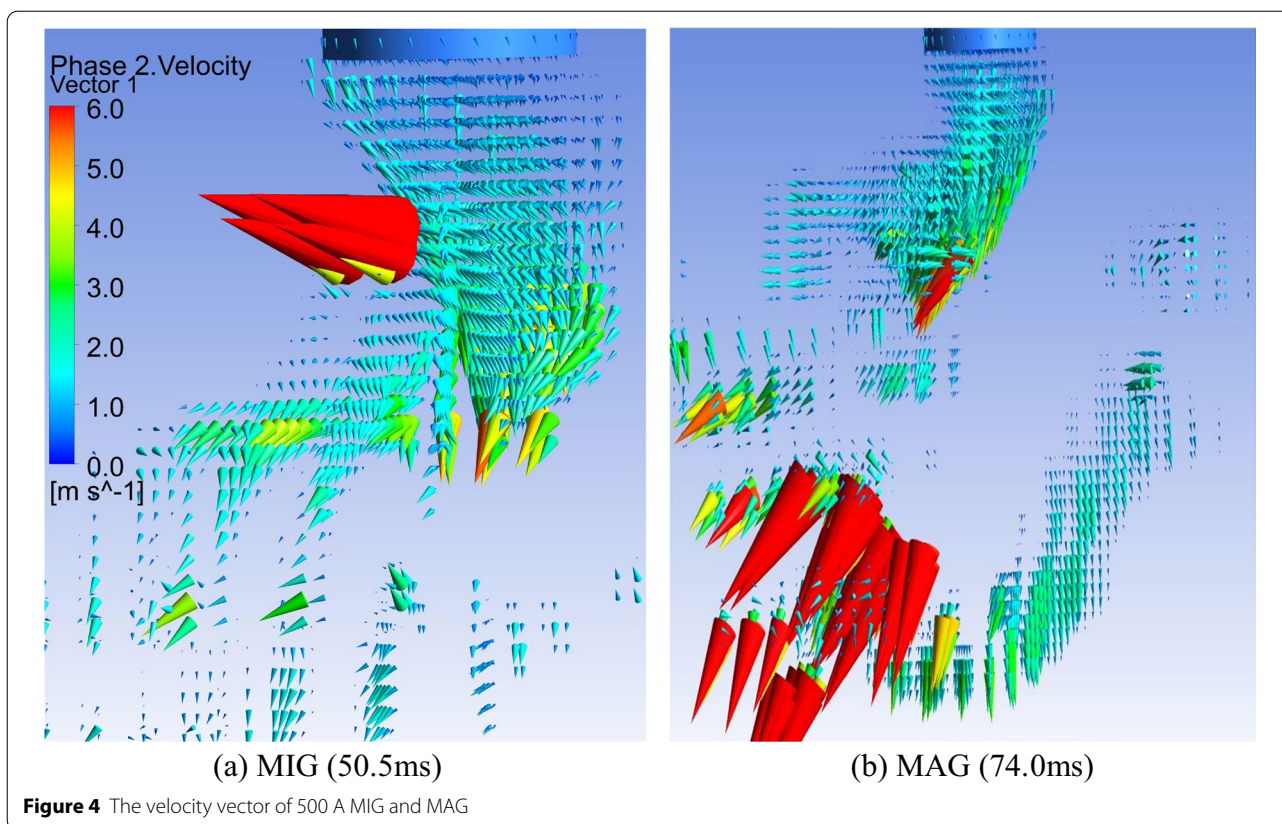
swing mechanism, the force analysis including gravity, electromagnetic force, surface tension force, and arc pressure is necessary.
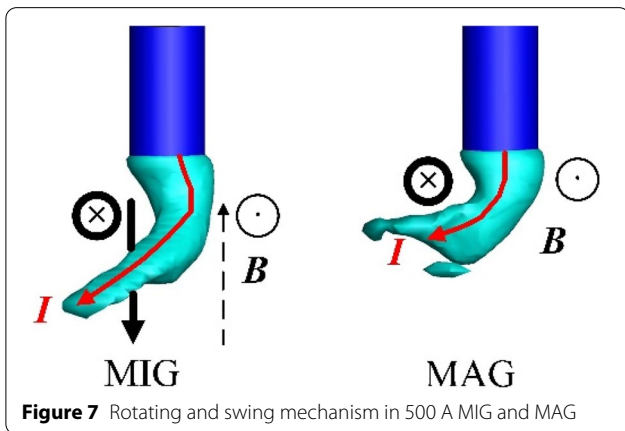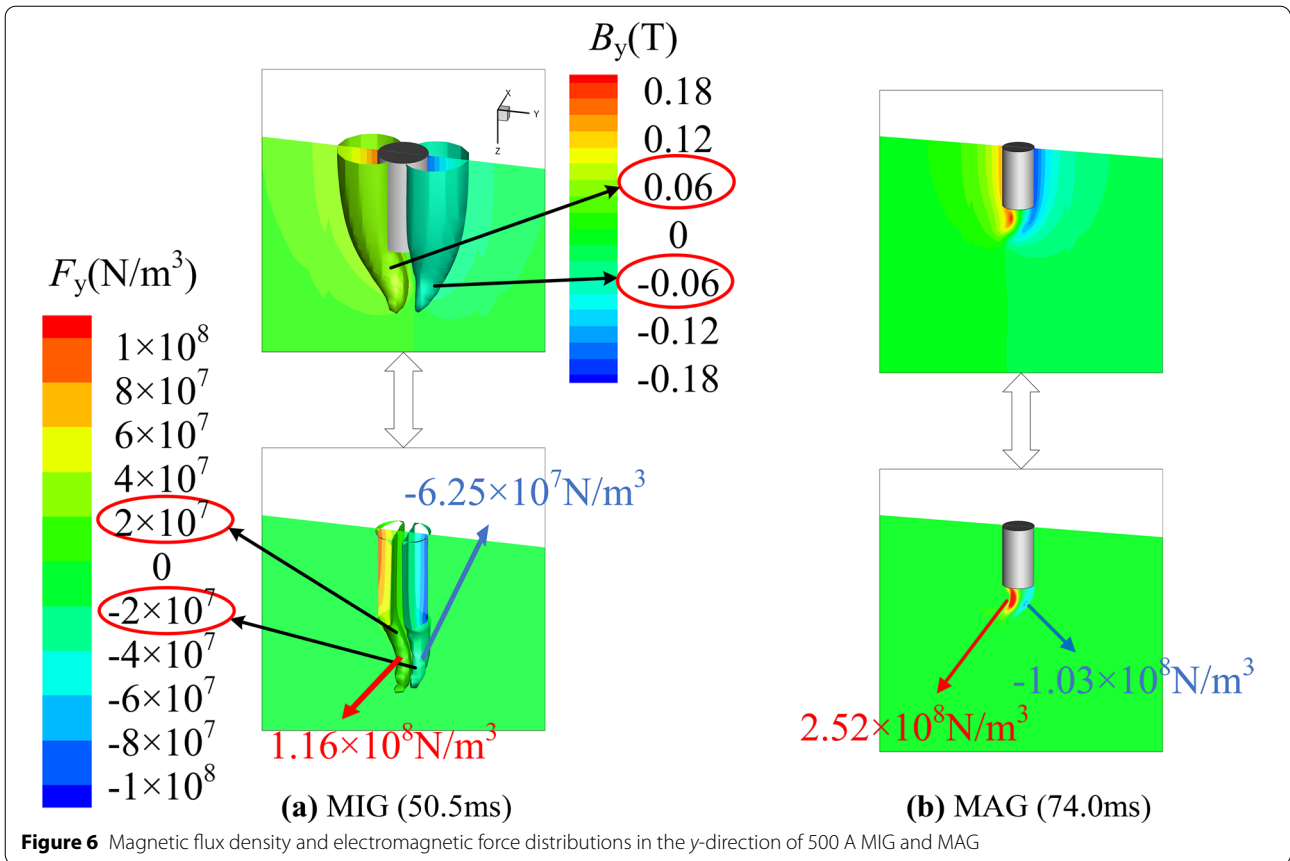
The electromagnetic force is the most powerful one for driving the metal liquid column to move because of the high current. The maximal current densities in the z-direction in one period of MIG/MAG are shown in Figure 5. It can be seen that the maximal current density in MAG has a larger amplitude. The conductivity in MAG arc is lower, hence more current flows through the metal liquid column, in which the current density is larger.

The self-induced magnetic flux density and electromagnetic force are shown in Figure 6. Observing at the contour surfaces of MIG, the magnetic flux density magnitude is larger on the concave side and lower on the convex side because the conductive path is inflected in the metal liquid column. And so does the self-induced magnetic flux density and electromagnetic force, which

(a) MIG (50.5ms)   (b) MAG (74.0ms)

Figure 4 The velocity vector of 500 A MIG and MAG

Figure 5 Maximal current density in the z-direction of 500 A MIG and MAG

is a pinch force. we should consider both the positive and negative electromagnetic force. According to the electromagnetic force source term of the momentum conservation equation, the larger magnetic flux density and current density on the concave side will lead to a larger electromagnetic force. At the first moment of 50.5 ms, the maximal positive electromagnetic force is about 1.16×10^8 N/m^3, and the maximal negative force on the opposite side is about -6.25×10^8 N/m^3. Finally, the resultant force with considering the force of both sides can push the metal liquid column to rotate. Observing at 74.0 ms of MAG, which has a larger resultant force with considering positive one of 2.52×10^8 N/m^3 and the negative one of -1.03×10^8 N/m^3. The larger resultant electromagnetic force will destroy the rotating motion. The current path and self-induced magnetic flux density are described in Figure 7. As shown in Figure 7 for MIG, the electromagnetic force is smaller with a spiral current path, therefore the current density has three components of axial, radial, and angular directions. The axial and radial current density can induce only the angular magnetic field, which is larger inside the spiral and smaller outside the spiral. The angular current density induces an axial magnetic field as shown as arrows in Figure 7 left, and the current density and induced magnetic flux density inside is also larger than the outside one. The maximal axial magnetic flux density inside the spiral is about 0.08 T, while it is 0.05 T in a negative direction outside. So the rotating motion can be continuous in the MIG case. For the case of MAG, when the electromagnetic force is larger than MIG, the larger

Figure 6 Magnetic flux density and electromagnetic force distributions in the *y*-direction of 500 A MIG and MAG

Figure 7 Rotating and swing mechanism in 500 A MIG and MAG

asymmetry electromagnetic force breaks the rotating motion and shifts it to a swing motion. As shown in Figure 7 right, it is different that there is only an angular induced magnetic field since there is no angular current density. The self-induced magnetic flux density on the curve side is no doubt larger than the other side, hence the unbalanced pinch force will push the metal liquid

column back to the other side, and then move back and forth. These are two metal transfer modes of melted metal in high-current GMAW.

We have considered the surface tension force using the continuum surface force model. The maximal surface tension forces along *y*-direction at 50.5 ms of MIG and 74.0 ms of MAG are respectively 1.1×10^8 N/m^3 and 1.2×10^8 N/m^3, as shown in Figure 8. The bending angle is 90° in MAG, so the surface tension force is small on the concave surface and larger on the convex surface, which will resist the swing motion. In this work, the surface tension coefficient of MIG and MAG is set to 1.2 N/m, which is independent of temperature and shielding gas environment. The surface tension coefficient of melted mild steel in active shielding gas condition is about 10%–15% lower than pure argon shielding gas [30]. Also, the Marangoni force caused by the temperature gradient is a strong acting force on the boundary of the gas and liquid phase. According to Cobine et al. [31] and Nemchinsky [32, 33], heavy vaporization occurs on the droplet surface. Hence, measurement and modeling of the Marangoni effect are very difficult. The other reason we have ignored the variational surface tension coefficient is that the electromagnetic force in this work is very

Figure 8 Surface tension forces along the y-direction of 500 A MIG and MAG
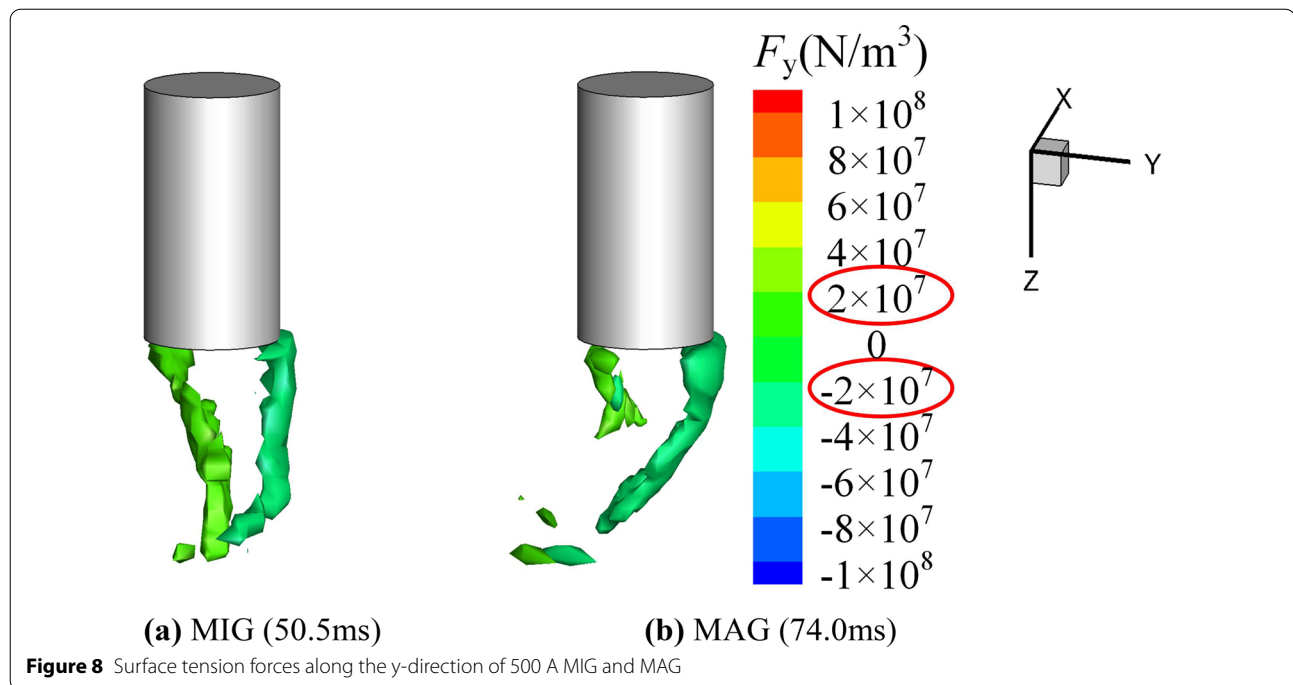
large. The swing motion will be intensified if we consider the surface tension coefficient decreasing in MAG. The surface tension force distributes on the boundary between the gas and the liquid phase where $0 < F_{mp} < 1$. Gravity is a volume force acting everywhere in the liquid phase, however, it is a constant of about 7.05×10^4 N/m^3, which is independent of anything and there is no difference between MIG and MAG.

Another acting force during the GMAW metal transfer is the plasma static pressure acting on the liquid phase surface of the interface boundary between the gas and liquid phase. According to the governing equation of momentum, the source term of electromagnetic forces can increase the arc static pressure. Figures 9 and 10 show the static pressure and flow field of arc plasma in 500 A MIG and MAG. For MIG, the maximal pressure force on the interface boundary reaches nearly 1.5×10^7 N/m^3 at 52.0 ms, which is of course much less than the maximal electromagnetic force and surface tension there. However, the pressure force is not a pinch force, and it turns to a promoting force directly without subtracting any opposite parts. As shown in the gas phase region of Figure 9b, the static pressure gradient in the arc plasma pushes the arc to flow under the metal flow beam, meanwhile the static pressure transfers to dynamic pressure, so the maximal gas velocity increases to nearly 700 m/s. At the beginning of the promotion, there is a large static pressure area that will hold the metal liquid column and impede the column to move through the

axis, hence the metal liquid column, under the promotion of the electromagnetic force, can only rotate around the axis. For MAG, the maximal arc pressure is about 2.9×10^7 N/m^3 at 76.0 ms, which is a relatively larger force than MIG. However, the unbalanced electromagnetic force is quite a strong controlling force to overcome the arc pressure to achieve swing motion. It can be seen in Figure 9 that the arc deflecting angle increases caused by the swing spray transfer process.

3.2 Experimental Results
We use a high-speed video camera (Olympus i-SPEED 3), a microlens (Nikon AF Micro 200 mm) attached with a band-pass filter with the nominal center wavelength of 650 ± 10 nm. The frame rate is set to 5000 f/s with a resolution of 804×600 pixels. The exposure parameters are selected based on the clear vision of both arc and droplet forms. The rotating deflected angles are measured as Figure 11 shows.

A mild steel filler wire with a diameter of 1.2 mm is used and the wire feeding rate is 30 m/min. The preset welding voltage is 50 V, and the contact tip to work distance (CTWD) is 30 mm. The arc length is different between MIG (pure argon shielding gas) and MAG (10% CO_2 mixed with argon) since they have the same preset welding voltage. Observational results of metal liquid column shape and rotating frequency (or swing frequency) are clearly shown in Figure 12. The welding current is about 450–550 A, which is influenced by the

(a) Arc pressure iso-surface of 1000Pa and -200Pa

(b) Arc flow field (52.0ms)

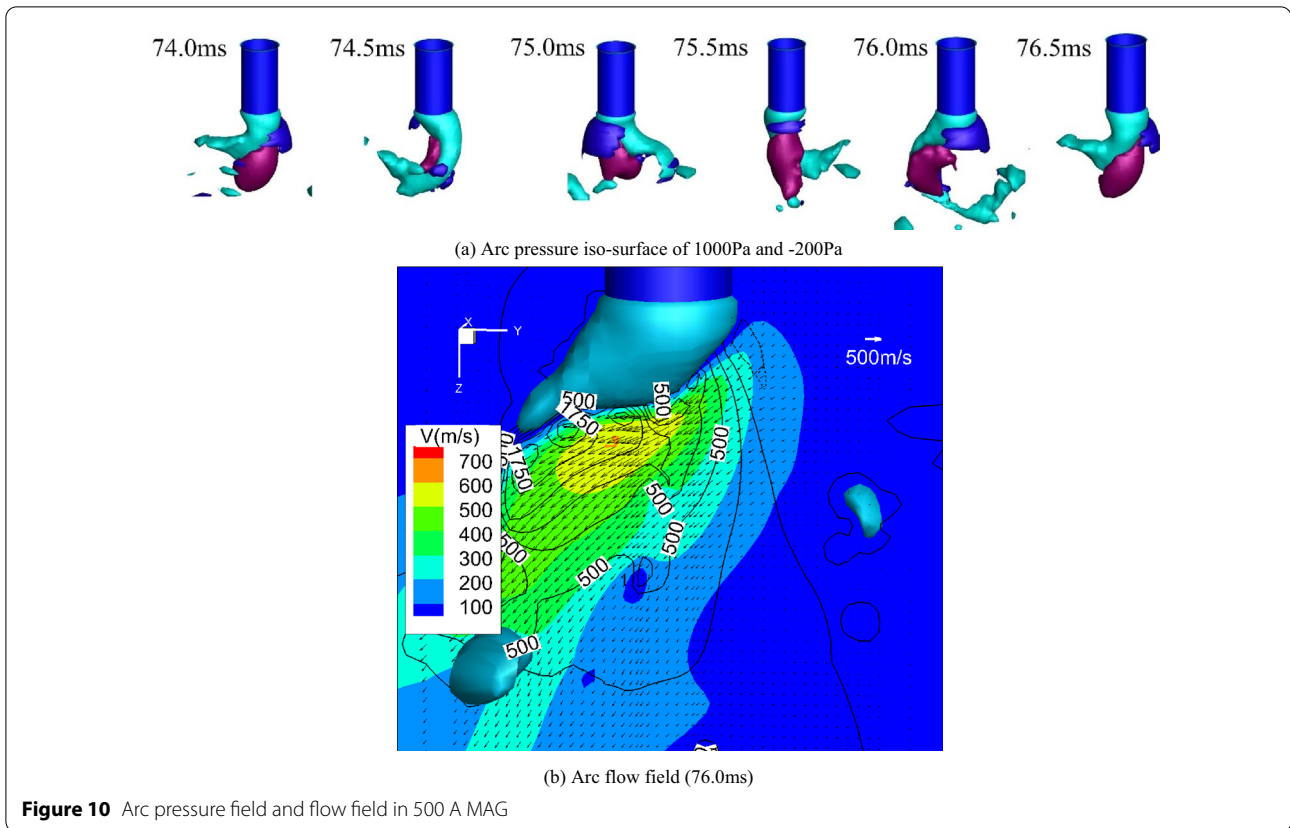**Figure 9** Arc pressure field and flow field in 500 A MIG
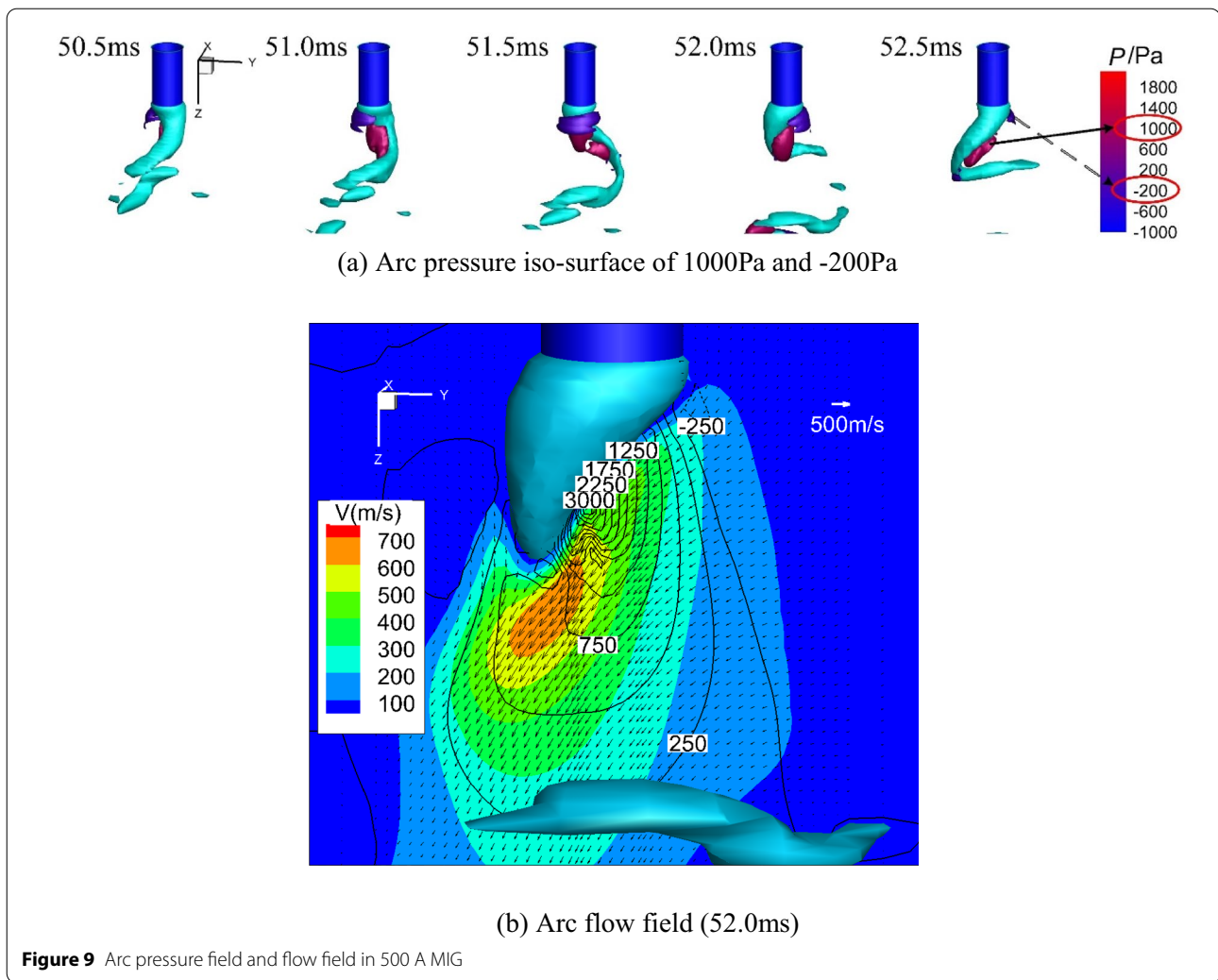
wire feeding stability. In Figure 12a, the metal liquid column rotates at the frequency of about 500 Hz, and the deflected angle in the front view of 0.2 ms is about 34°, comparing with that in Figure 3a, at 52.5 ms, the deflected angle is about 35°. In Figure 12b, the swing frequency is about 450 Hz, and the maximal deflected angle is approximate 90° as same as the calculated deflected angle.

3.3 Discussion

The current path is very important for the calculated results of the electromagnetic force. It is easily affected by the arc attachment to the metal liquid column. However, there are a lot of difficult problems for the numerical study of the arc-metal coupled behavior with considering mass, momentum, and heat transfer process since the anode sheath boundary is extremely complicated. In this work, we remove the energy conservation equation to simplify our mathematic model for a more complex

high-current GMAW metal transfer process. The arc properties depend on the arc temperature which is not calculated, therefore the fixed arc conductivity, density, viscosity are assumed. To ensure the accuracy of the calculation, we choose the arc physical properties and transfer properties as the argon plasma properties at about 15000 K. We should point out that it is just a simplified acting forces model of the metal liquid column for high-current GMAW metal transfer. Actually, according to Ref. [22], it was reported that the metal vapor influenced the current path a lot. Most of the current flows through the region where there is no metal vapor, hence the current density should decrease at the metal liquid column tip comparing with our model.

In this section, the metal rotating spray and swing spray transfer mechanism is discussed. The unbalanced electromagnetic forces are presumed to be important factors for the metal transfer mechanism of high-current GMAW. For MIG welding with pure argon

(a) Arc pressure iso-surface of 1000Pa and -200Pa

(b) Arc flow field (76.0ms)

**Figure 10** Arc pressure field and flow field in 500 A MAG

shielding gas, the arc expands and more current flows through the arc region instead of the metal liquid column, hence the current density in the metal is lower than that in MAG with Ar-CO$_2$ mixing shielding gas. The metal liquid column will be kinky under the asymmetric electromagnetic forces whatever it is MIG or MAG. However, the resultant force of asymmetric electromagnetic forces is smaller in MIG and larger in MAG as shown in Figure 6. When the resultant force of asymmetric electromagnetic forces is small, the metal liquid column deflected angle is an acute angle, and the

Figure 11 Metal rotating angle measurement schematic diagram
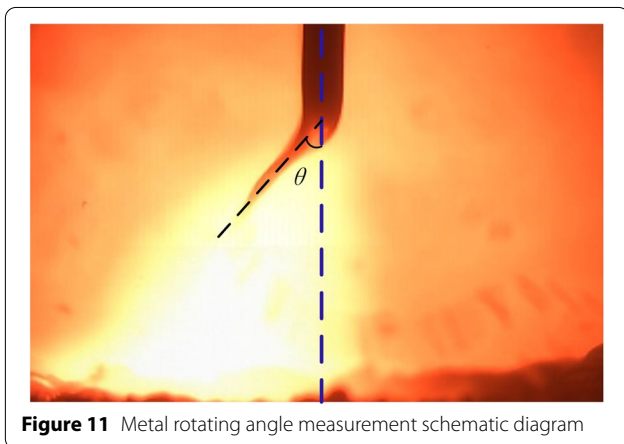
metal liquid column has a spiral structure, in which, the current density will generate a self-induced axial magnetic field. The spiral motion can be maintained with the help of self-induced angular force coming from the multiplication of the axial magnetic flux density and radial current density. To control the rotating motion of the MIG case, an additional negative and cyclically varying axial magnetic field for counteracting the self-induced axial magnetic field is expectant. When the resultant force of asymmetric electromagnetic forces is large in the MAG case, the metal liquid column deflected angle is no longer an acute angle. The large promoting force can destroy the rotating motion and spiral structure. Hence the liquid column has a plane structure, in which, the current density can only induce the magnetic field along the transverse direction. With the help of a cyclically varying induced transverse magnetic field, the metal liquid column will swing back and forth. To control the swing motion of the MAG case, the additional negative and cyclically varying transverse magnetic field for counteracting the self-induced axial magnetic field is expectant.

It is shown that the arc pressure attached to the metal liquid column is another important acting force for metal transfer of high-current GMAW. According to

Figure 12 Experimentally observing metal transfer processes of MIG and MAG
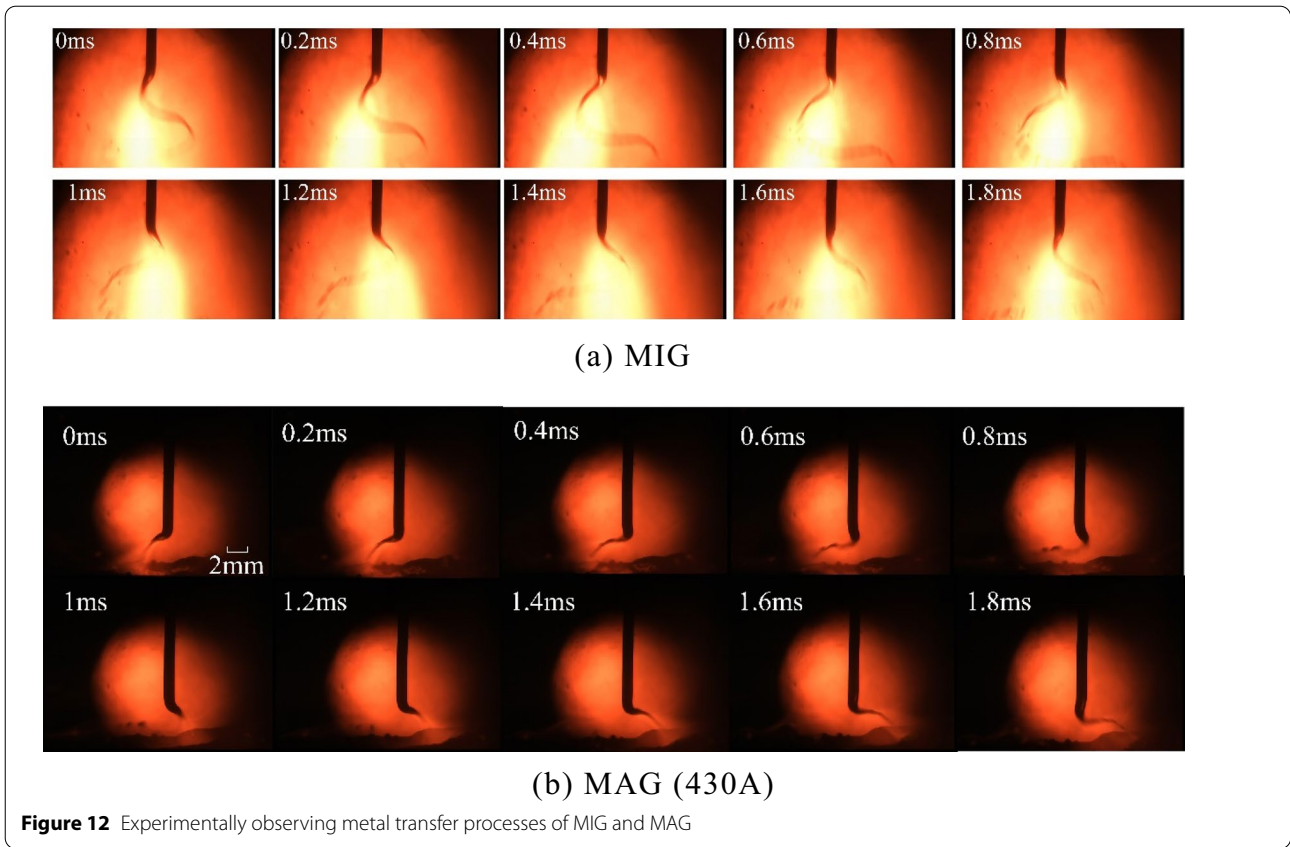
the calculated results without considering arc flow, it is to say that we remove the electromagnetic force source in the gas phase region. The calculated results of the metal transfer process are displayed in Figure 13. It can be seen that the liquid column stops its rotating motion
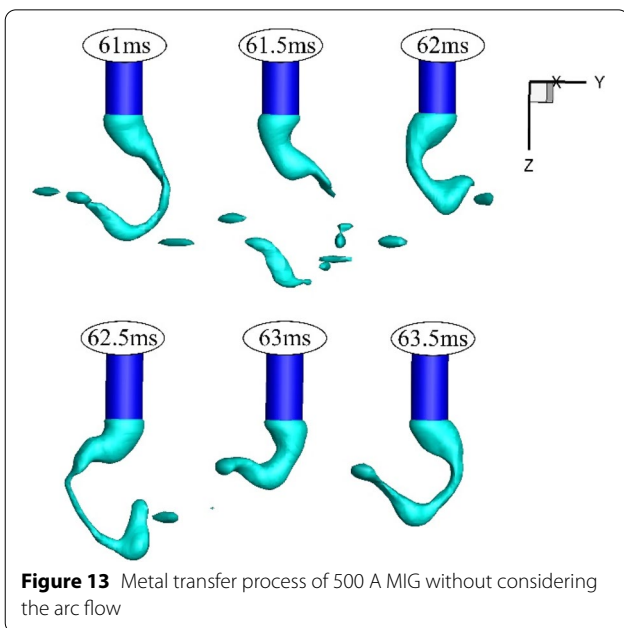

Figure 13 Metal transfer process of 500 A MIG without considering the arc flow

and changes to swing with a deflected angle of about 30°. Since the arc static pressure prevents the liquid column to swing across the z-axis where the arc static pressure reaches its maximal value, the metal liquid column can only change its moving path beside the z-axis as a spiral structure. The strong arc pressure is probably one of the main reasons why there are swing and rotating spray transfer models in high-current GMAW processes. In Ref. [25], without considering the arc pressure, the calculated results about the metal transfer process of high-current GMAW showed that the metal liquid column would swing under the unbalanced electromagnetic pinch force.

4 Conclusions

(1) There are two metal transfer modes in high-current GMAW, rotating spray transfer and swing spray transfer. In the 500 A MIG welding process, less current flows through the melted metal, the unbalanced pinch force can push the metal liquid column to rotate. However, in the 500 A MAG welding process, more current flows through the melted metal, the large unbalanced electromagnetic

Xiao *et al. Chinese Journal of Mechanical Engineering*   (2022) 35:131

Page 12 of 13

pinch force will destroy the rotating motion and turn to swing.

(2) The spiral structure of the rotating spray transfer process generates an induced axial magnetic field, which could also stabilize the rotating motion. To control the rotating motion of the MIG case, an additional negative axial magnetic field for counteracting the self-induced axial magnetic field is expectant. The flat structure of the swing spray transfer process can only generate the transverse magnetic field to stabilize the swing motion. To control the swing motion of the MAG case, the additional negative and cyclically varying transverse magnetic field for counteracting the self-induced axial magnetic field is expectant.

Authors' Contributions
DF was in charge of the whole trial; LX wrote the manuscript; JH assisted with modeling and experimental analyses. All authors read and approved the final manuscript.

Authors' Information
Lei Xiao, born in 1991, is currently a lecturer at *Lanzhou Jiaotong University, China*. He received his doctor degree from *Lanzhou University of Technology, China*, in 2020. His research interests include high-efficiency welding technology and numerical simulation. Tel: +86-931-4955788.
Ding Fan, born in 1961, is currently a professor at *Lanzhou University of Technology, China*. He received his master degree from *Xi'an Jiaotong University, China*, in 1984. His research interests include high-efficiency welding technology, welding process control and numerical simulation. Tel: +86-931-2976378.
Jiankang Huang, born in 1981, is currently a professor at *Lanzhou University of Technology, China*. He received his PhD degree from *Lanzhou University of Technology, China*, in 2010. His research interests include welding process control and numerical simulation. Tel: +86-931-2976378.

Competing Interests
The authors declare no competing financial interests.

Author Details
[1]School of Materials Science and Engineering, Lanzhou Jiaotong University, Lanzhou 730070, China. [2]State Key Laboratory of Advanced Processing and Recycling of Non-ferrous Metals, Lanzhou University of Technology, Lanzhou 730050, China. [3]School of Materials Science and Engineering, Lanzhou University of Technology, Lanzhou 730050, China.

References
[1]   J F Lancaster. *The physics of welding*. Oxford: Pergamon Press, 1984.
[2]   P K J Mistry. Impact of welding processes on environment and health. *International Journal of Advanced Research in Mechanical Engineering & Technology*, 2015, 1: 17-20.
[3]   C Shu, J Wang, W Hui, et al. Principle of rotating transfer undergoing longitudinal magnetic field control. *Transactions of the China Welding Institution*, 2005.
[4]   W Hong, Y Chang, L Lin, et al. Review on magnetically controlled arc welding process. *International Journal of Advanced Manufacturing Technology*, 2017, 91: 4263-4273.
[5]   H Baba, T Era, T Ueyama, et al. Single pass full penetration joining for heavy plate steel using high current GMA process. *Welding in the World*, 2017, 61: 1-7.
[6]   W J Greene. An analysis of transfer in gas-shielded welding arcs. *Transactions of the American Institute of Electrical Engineers Part II Applications & Industry*, 1960, 79: 194-203.
[7]   J C Amson. Lorentz force in the molten tip of an arc electrode. *British Journal of Applied Physics*, 1965, 16: 1169-1179.
[8]   C J Allum. Metal transfer in arc welding as a varicose instability. *Journal of Applied Physics*, 1985, 18: 1447-1468.
[9]   C J Allum. Metal transfer in arc welding as a varicose instability. I. Varicose instabilities in a current-carrying liquid cylinder with surface charge. *Journal of Physics D: Applied Physics*, 2000, 18: 1431.
[10]   S Choi, C Yoo, Y Kim. Dynamic simulation of metal transfer in GMAW, part 1: Globular and spray transfer modes. *Welding Journal*, 1998, 77: 38-s.
[11]   G Wang, P Huang, Y Zhang. Numerical analysis of metal transfer in gas metal arc welding under modified pulsed current conditions. *Metallurgical and Materials Transactions B*, 2004, 35: 857-866.
[12]   M Chen, C S Wu, R Lian. Numerical analysis of dynamic process of metal transfer in GMAW. *Acta Metallrugica Sinica*, 2004, 40: 1227-1232.
[13]   F Wang, W K Hou, S J Hu, et al. Modelling and analysis of metal transfer in gas metal arc welding. *Journal of Physics D: Applied Physics*, 2003, 36: 1143-1152(1110).
[14]   J Haidar, J J Lowke. Predictions of metal droplet formation in arc welding. *Journal of Physics D: Applied Physics*, 1996, 29: 2951.
[15]   J Hu, H L Tsai. Heat and mass transfer in gas metal arc welding. Part I: The arc. *International Journal of Heat & Mass Transfer*, 2007, 50: 833-846.
[16]   G Xu, J Hu, H L Tsai. Three-dimensional modeling of arc plasma and metal transfer in gas metal arc welding. *International Journal of Heat & Mass Transfer*, 2009, 52: 1709-1724.
[17]   M Hertel, A Spille-Kohoff, U Füssel, et al. Numerical simulation of droplet detachment in pulsed gas metal arc welding including the influence of metal vapour. *Journal of Physics D: Applied Physics*, 2013, 46: 4003.
[18]   Y Ogino, Y Hirata. Numerical simulation of metal transfer in argon gas-shielded GMAW. *Welding in the World*, 2015, 59: 1-9.
[19]   Y Ogino, Y Hirata, A B Murphy. Numerical simulation of GMAW process using Ar and an Ar-CO₂ gas mixture. *Welding in the World*, 2016, 60: 1-9.
[20]   S Tashiro, A B Murphy, M Tanaka. Numerical simulation of fume formation process in GMA welding. *Welding in the World, Le Soudage Dans Le Monde*, 2018, 62: 1331-1339.
[21]   M Boselli, V Colombo, E Ghedini, et al. Time-dependent modeling of droplet detachment in GMAW including metal vapor diffusion. *IEEE Transactions on Plasma Science*, 2011, 39: 2896-2897.
[22]   M Hertel, M Trautmann, S Jäckel, et al. The role of metal vapour in gas metal arc welding and methods of combined experimental and numerical process analysis. *Plasma Chemistry & Plasma Processing*, 2017, 37: 531-547.
[23]   J Haidar. Predictions of metal droplet formation in gas metal arc welding. II. *Journal of Applied Physics*, 1998, 84: 3530-3540.
[24]   J Haidar. An analysis of the formation of metal droplets in arc welding. *Journal of Physics D: Applied Physics*, 1999, 31: 1233-1244.
[25]   Y Ogino, Y Hirata, S Kihana, et al. Numerical simulation of free-flight transfer by a 3D metal transfer model. *Quarterly Journal of the Japan Welding Society*, 2018, 36: 94-103.
[26]   J Hu, H L Tsai. Heat and mass transfer in gas metal arc welding. Part II: The metal. *International Journal of Heat & Mass Transfer*, 2007, 50: 808-820.
[27]   J U Brackbill, D B Kothe, C Zemach. A continuum method for modeling surface tension. *J. Comp. Phys.*, 1992, 100: 335-354.
[28]   J J Lowke, M Tanaka. 'LTE-diffusion approximation' for arc calculations. *Journal of Physics D: Applied Physics*, 2006, 39: 3634.
[29]   K Nomura, K Yoshii, K Toda, et al. 3D measurement of temperature and metal vapor concentration in MIG arc plasma using a multidirectional

spectroscopic method. *Journal of Physics D Applied Physics*, 2017, 50: 425205.

[30] P Sahoo, T Debroy, M J Mcnallan. Surface tension of binary metal—surface active solute systems under conditions relevant to welding metallurgy. *Metallurgical Transactions B*, 1988, 19: 483-491.

[31] J D Cobine, E E Burger. Analysis of electrode phenomena in the high-current arc. *Journal of Applied Physics*, 1955, 26: 895.

[32] Nemchinsky, V A. Electrode evaporation in an arc with pulsing current. *Journal of Physics D: Applied Physics*, 1997, 30: 2895-2899.

[33] Nemchinsky, V A. Heat transfer in a liquid droplet hanging at the tip of an electrode during arc welding. *Journal of Physics D: Applied Physics*, 1997, 30: 1120-1124.